Controls on Dense Shelf Water formation in four East Antarctic polynyas

Esther Portela Rodriguez, Stephen Rintoul, Laura Herraiz-Borreguero, Fabien Roquet, Sophie Bestley, Esmee van Wijk, Takeshi Tamura, Clive Mcmahon, Christophe Guinet, Robert Harcourt, et al.

▶ **To cite this version:**

Esther Portela Rodriguez, Stephen Rintoul, Laura Herraiz-Borreguero, Fabien Roquet, Sophie Bestley, et al.. Controls on Dense Shelf Water formation in four East Antarctic polynyas. Journal of Geophysical Research. Oceans, 2022, 127. hal-03659459v2

HAL Id: hal-03659459
https://hal.science/hal-03659459v2

Submitted on 15 Oct 2024

HAL is a multi-disciplinary open access archive for the deposit and dissemination of scientific research documents, whether they are published or not. The documents may come from teaching and research institutions in France or abroad, or from public or private research centers.

L'archive ouverte pluridisciplinaire **HAL**, est destinée au dépôt et à la diffusion de documents scientifiques de niveau recherche, publiés ou non, émanant des établissements d'enseignement et de recherche français ou étrangers, des laboratoires publics ou privés.

Distributed under a Creative Commons Attribution - NonCommercial - NoDerivatives 4.0 International License

Check for updates

JGR Oceans

RESEARCH ARTICLE
10.1029/2022JC018804

Controls on Dense Shelf Water Formation in Four East Antarctic Polynyas

Esther Portela[1,2], Stephen R. Rintoul[3,4,5], Laura Herraiz-Borreguero[3,5], Fabien Roquet[6], Sophie Bestley[1,4], Esmee van Wijk[3,4], Takeshi Tamura[7,8], Clive R. McMahon[1,9], Christophe Guinet[10], Robert Harcourt[11], and Mark A. Hindell[1]

[1]Institute for Marine and Antarctic Studies, University of Tasmania, Hobart, TAS, Australia, [2]University of Brest, Laboratoire d'Océanographie Physique et Spatiale, CNRS, IRD, Ifremer, Plouzané, France, [3]Commonwealth Scientific and Industrial Research Organization (CSIRO) Environment, Hobart, TAS, Australia, [4]Australian Antarctic Program Partnership, Institute for Marine and Antarctic Studies, University of Tasmania, Nipaluna/Hobart, TAS, Australia, [5]Centre for Southern Hemisphere Oceans Research Centre (CSHOR), Hobart, TAS, Australia, [6]Department of Marine Sciences, University of Gothenburg, Gothenburg, Sweden, [7]National Institute of Polar Research, Tachikawa, Japan, [8]Graduate University for Advanced Studies (SOKENDAI), Tachikawa, Japan, [9]Integrated Marine Observing System Animal Tagging Sub-Facility, Sydney Institute of Marine Science, Mosman, NSW, Australia, [10]Centre d'Etude Biologiques de Chizé UMR 7372, La Rochelle Université, CNRS, Villiers en Bois, France, [11]School of Natural Sciences, Macquarie University, Sydney, NSW, Australia

Key Points:

- We determined the physical factors enhancing (or hindering) dense shelf water (DSW) formation in four East Antarctic polynyas during a well sampled year
- Relatively high salinity in early winter and high sea-ice formation favor DSW formation in Mackenzie Polynya
- The properties and volume of DSW formed in a coastal polynya depend on its preconditioning as well as on sea-ice formation

Supporting Information:

Supporting Information may be found in the online version of this article.

Correspondence to:

E. Portela,
eportelanh@gmail.com

Citation:

Portela, E., Rintoul, S. R., Herraiz-Borreguero, L., Roquet, F., Bestley, S., van Wijk, E., et al. (2022). Controls on dense shelf water formation in four East Antarctic polynyas. *Journal of Geophysical Research: Oceans*, *127*, e2022JC018804. https://doi.org/10.1029/2022JC018804

Received 28 APR 2022
Accepted 15 NOV 2022

© 2022. The Authors.
This is an open access article under the terms of the Creative Commons Attribution-NonCommercial-NoDerivs License, which permits use and distribution in any medium, provided the original work is properly cited, the use is non-commercial and no modifications or adaptations are made.

Abstract

Coastal polynyas are key formation regions for dense shelf water (DSW) that ultimately contributes to the ventilation of the ocean abyss. However, not all polynyas form DSW. We examine how the physiographic setting, water-mass distribution and transformation, water column stratification, and sea-ice production regulate DSW formation in four East Antarctic coastal polynyas. We use a salt budget to estimate the relative contribution of sea-ice production and lateral advection to the monthly change in salinity in each polynya. DSW forms in Mackenzie polynya due to a combination of physical features (shallow water depth and a broad continental shelf) and high sea-ice production. Sea-ice formation begins early (March) in Mackenzie polynya, counteracting fresh advection and establishing a salty mixed layer in autumn that preconditions the water column for deep convection in winter. Sea-ice production is moderate in the other three polynyas, but saline DSW is not formed (a fresh variety is formed in the Barrier polynya). In the Shackleton polynya, brine rejection during winter is insufficient to overcome the very fresh autumn mixed layer. In Vincennes Bay, a strong inflow of modified Circumpolar Deep Water stratifies the water column, hindering deep convection and DSW formation. Our study highlights that DSW formation in a given polynya depends on a complex combination of factors, some of which may be strongly altered under a changing climate, with potentially important consequences for the ventilation of the deep ocean, the global meridional overturning circulation, and the transport of ocean heat to Antarctic ice shelves.

Plain Language Summary

Coastal polynyas are regions of open water surrounded by sea ice. As sea ice forms, it is pushed offshore by strong winds blowing from the Antarctic continent, keeping the polynya ice-free. Salt is released into the water below as sea ice forms, increasing the salinity and density of the water column. In some polynyas, this water is dense enough to sink from the continental shelf to supply a network of bottom ocean currents that influences global climate. In other polynyas, the water in winter never gets dense enough to reach the ocean abyss. Using data collected by instrumented elephant seals, we investigated the main factors controlling dense water formation in four East Antarctic polynyas. We found that dense water production is related to the strength of sea-ice formation, as expected, but also depends on the salinity at the start of winter. The geographical and physical characteristics of the polynyas and regional circulation also modulate the final water density. Our findings provide insight into how dense water formation in East Antarctic polynyas might respond to future changes in climate and thereby influence the transport of ocean heat to the Antarctic continent and the melt of ice shelves.

1. Introduction

Coastal polynyas are regions of open water or low sea ice concentration where the ocean surface is directly exposed to the cold atmosphere. Persistent wind-driven sea ice export and winter heat loss in coastal polynyas results in continuous sea ice formation and brine rejection. In some polynyas, the buoyancy loss due to cooling

21699291, 2022, 12, Downloaded from https://agupubs.onlinelibrary.wiley.com/doi/10.1029/2022JC018804 by Cochrane France, Wiley Online Library on [15/10/2024]. See the Terms and Conditions (https://onlinelibrary.wiley.com/terms-and-conditions) on Wiley Online Library for rules of use; OA articles are governed by the applicable Creative Commons License

and salinification is sufficient to drive deep convection and formation of dense shelf water (DSW).

The cold and salty DSW that cascades down the Antarctic continental slope is the precursor of Antarctic Bottom Water (AABW), the densest water mass in the ocean. The down-slope transport of DSW and AABW formation play a crucial role in Earth's climate system, global deep-ocean circulation (Jacobs, 2004; Orsi et al., 1999), and biogeochemical cycles (Shapiro et al., 2003). They connect the surface waters, imprinted with the signal of exchange with the atmosphere, with the deep ocean and transport dense water and tracers toward lower latitudes, ventilating the ocean abyss (Foster & Carmack, 1976; Orsi et al., 2002).

The two major sites of AABW formation around Antarctica are the Weddell Sea and Ross Sea (Orsi et al., 2002). These regions host highly productive coastal polynyas on wide continental shelves with large neighboring ice shelves and cross-shelf depressions that have the capacity to accumulate and export large volumes of DSW (Gordon et al., 2004). In contrast, the Adélie Land source region in East Antarctica is located on a narrower continental shelf with more limited storage capacity, where the persistent Mertz polynya activity drives a relatively fresh Bottom Water supply (Gordon & Tchernia, 1972; Rintoul, 1998; Williams et al., 2008). More recently, the Cape Darnley-Prydz Bay region has been identified as another region exporting DSW to form AABW (Herraiz-Borreguero et al., 2015, 2016; Ohshima et al., 2013; Portela et al., 2021; Williams et al., 2016). While these studies highlight the role of coastal polynyas in the formation of these dense-water overflows, DSW is noticeably absent in other coastal polynyas (Narayanan et al., 2019; Ribeiro et al., 2021; Silvano et al., 2018).

Previous studies have assessed the influence of cryospheric, oceanographic, and physiographic factors (Amblas & Dowdeswell, 2018; Baines & Condie, 1998; Narayanan et al., 2019) on DSW formation and export. While the primary mechanism for DSW formation is high sea-ice production and consequent salt rejection in coastal polynyas, physiographic factors (e.g., polynya size and depth, topography, and shelf geography), regional circulation, and the water masses present on the shelf likely modulate the production of DSW (Amblas & Dowdeswell, 2018; Liu et al., 2018; Narayanan et al., 2019; Portela et al., 2021). However, little is known about these interactions and their influence on DSW formation. The absence of DSW in some polynyas has been attributed to the inflow of warm modified Circumpolar Deep Water (mCDW) onto the shelves leading to high basal melt rates of the adjoining glaciers (Narayanan et al., 2019; Ribeiro et al., 2021; Williams et al., 2016). The resulting freshwater outflow increases the stratification of the water column, hinders vertical convection and can thereby suppress the formation of DSW on the continental shelf (Silvano et al., 2018). The increased stratification inhibits deep convection, allowing mCDW intrusions below the depth of convection to reach the calving front without loss of heat to the atmosphere (Silvano et al., 2017). The presence of DSW in a given polynya can influence the melt of nearby ice shelves in two ways. On the one hand, DSW has the potential to cause basal melt if it can access the grounding line, which is likely due to its high density. Due to the pressure dependence of the freezing point, the DSW is warmer than the in situ freezing point and therefore melts the underside of the ice shelf (Jacobs et al., 1992; Silvano et al., 2016). In addition, because DSW is denser than mCDW, the presence of DSW can also prevent warmer mCDW from reaching the grounding line (Jacobs et al., 1992), resulting in the lower basal melt.

A better understanding of the factors regulating DSW formation in coastal polynyas will provide insight into the sensitivity of AABW formation and basal melt of ice shelves to a changing climate. The few decades of available DSW overflow records show a reduction of DSW export in some areas around Antarctica (Amblas & Dowdeswell, 2018). This apparent weakening of DSW formation on the Antarctic continental shelves may partly explain the observed changes in AABW (e.g., warming, freshening and volume reduction (Fox-Kemper et al., 2021; Kobayashi, 2018; Purkey & Johnson, 2012; Van Wijk & Rintoul, 2014)). This link between DSW formation and the change in AABW characteristics highlights the variability of these complex ice-ocean systems and their potential vulnerability to climate change. Here, we use observations from four coastal polynyas in the particular year they were best sampled to investigate the factors that favor or restrict the formation of DSW. The well-sampled year we analyzed does not have to be necessarily representative of the long-term mean. Rather, we are interested in the question: "given that DSW formation was observed (or not observed) in a given polynya in a given year, what physical factors acted to enhance (or hinder) DSW formation there?". Our approach includes (a) investigation of water-mass transformation over winter, (b) assessment of the role of preconditioning and (c) computation of a salt budget to estimate the relative contribution of brine rejection and salt advection in driving observed monthly salinity changes. By comparing polynyas that do and do not produce DSW, we aim to gain an improved understanding of the physical processes that regulate DSW formation, now and in the future.

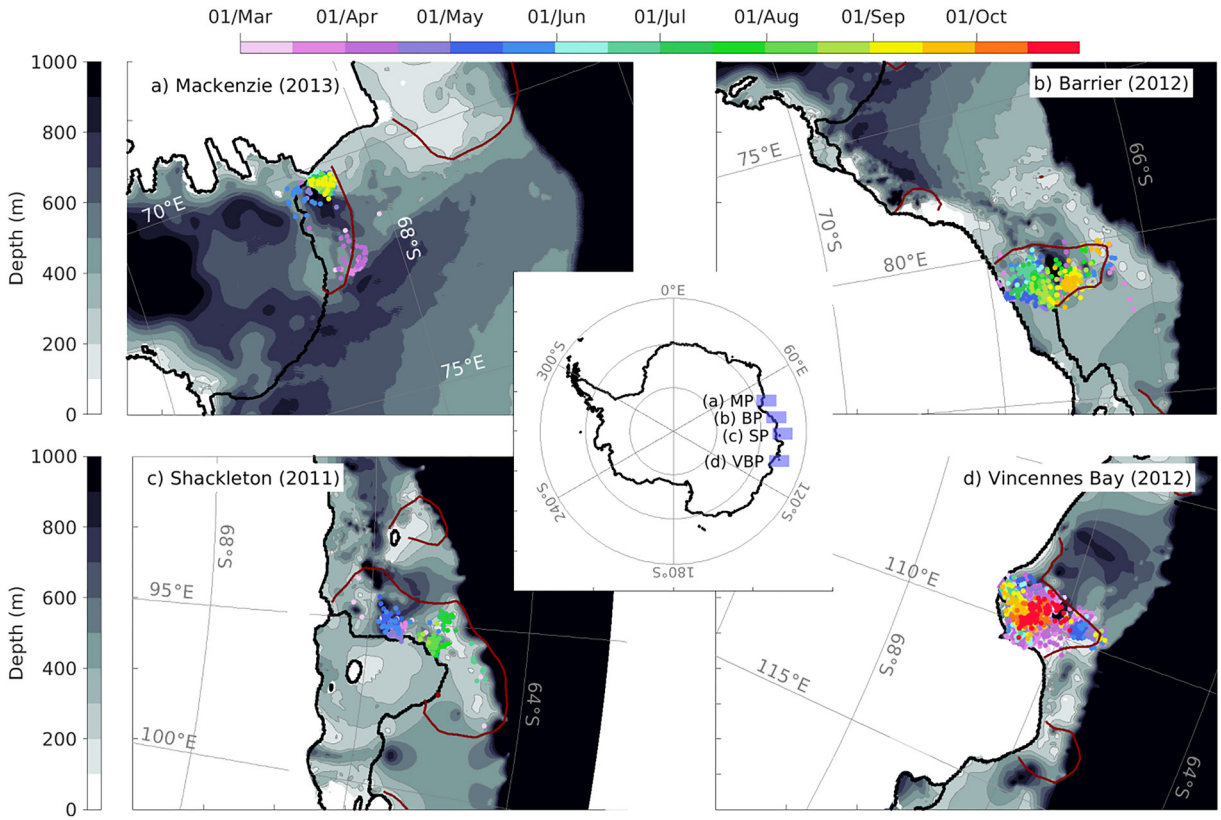

Figure 1. Location of vertical profile sampling (color-coded by time) within four East Antarctic coastal polynyas: (a) 2013 Mackenzie (MP), (b) 2012 Barrier (BP) (c) 2011 Shackleton (SP) and (d) 2012 Vincennes Bay (VBP). The polynya area is delimited by brown lines. The black contour delimits the coastline (white color) and the ice shelf fronts (colored by their bathymetry).

2. Methods

We analyzed four East Antarctic coastal polynyas: Mackenzie (MP), Barrier (BP), Shackleton (SP) and Vincennes Bay (VBP) (Figure 1). These polynyas were chosen because they have good temporal and spatial observational sampling by animal-borne sensors (Section 2.1) during autumn-winter and their characteristics span a range of sea ice formation rates, geographic settings, and water mass distributions. As shown below, in the years they were best sampled, MP was an active source of DSW, BP was a weak source of relatively light DSW, and SP and VBP produced little or no DSW.

2.1. Data

The vertical temperature-salinity profiles used in this study were collected by southern elephant seals (*Mirounga leonina*) instrumented with Conductivity-Temperature-Depth Satellite-Relayed Data Loggers (CTD-SRDLs) during their annual post-molt (February–October) foraging trips. Southern elephant seals are excellent Southern Ocean samplers (McMahon et al., 2021; Roquet et al., 2014), and in particular have provided almost all the available data within Antarctic coastal polynyas during winter (Labrousse et al., 2018; Malpress et al., 2017). The profile data were retrieved from the Marine Mammals Exploring the Oceans Pole to Pole (MEOP) database (http://www.meop.net/), which is a comprehensive quality-controlled database (Roquet et al., 2014) that is an essential component of the global ocean observing system. Additional data sources were explored, but the sampling of coastal polynyas by more traditional oceanographic platforms (e.g., ships, floats and moorings) is comparatively sparse and not suitable.

We investigate DSW formation by considering month-to-month changes in the salinity of the mixed layer. Therefore, for each polynya, we choose the year with the best sampling of the winter season. This means that data from different years are used in different polynyas: 2013 for MP, 2012 for BP and VBP, and 2011 for SP. As we are

21699291, 2022, 12, Downloaded from https://agupubs.onlinelibrary.wiley.com/doi/10.1029/2022JC018804 by Cochrane France, Wiley Online Library on [15/10/2024]. See the Terms and Conditions (https://onlinelibrary.wiley.com/terms-and-conditions) on Wiley Online Library for rules of use; OA articles are governed by the applicable Creative Commons License

21699291, 2022, 12, Downloaded from https://agupubs.onlinelibrary.wiley.com/doi/10.1029/2022JC018804 by Cochrane France, Wiley Online Library on [15/10/2024]. See the Terms and Conditions (https://onlinelibrary.wiley.com/terms-and-conditions) on Wiley Online Library for rules of use; OA articles are governed by the applicable Creative Commons License

interested in understanding the processes that influence DSW formation in each polynya during a particular year, the fact that different years are used in different polynyas is not relevant. The time series use profiles from a single seal in MP and in SP, two seals in BP, and 23 seals in VBP; the time of the sampling for each seal can be seen in Figure S1 in Supporting Information S1. The study area, as well as the location and date of the profiles collected by the tagged seals, is shown in Figure 1. Hereafter, all the analyses and comparisons refer to the selected year for each polynya.

To estimate the contribution of brine rejection to the salinity increase in each polynya, we calculated daily sea-ice production. Sea-ice production was derived from special sensor microwave/imager (SSM/I) and special sensor microwave imager/sounder (SSMI/S) data and atmospheric reanalysis from the ERA5 data set. Sea Ice Production (SIP) data are seamlessly available for 28 years between 1992 and 2019. This data set is similar to that of Tamura et al. (2016) but uses different atmospheric forcing (ERA5 data are used in this study instead of ERA-interim).

2.2. Polynya Identification

We identified polynyas using a combination of dynamic thin-ice thickness and static bathymetric data. The 12.5-km resolution twice-daily thin-ice thickness data set was obtained as described in Tamura et al. (2007). Detection and estimation of sea ice thicknesses between 0.01 and 0.2 m (considered as thin-ice) are based on the SSM/I 85- and 37-GHz polarization ratios (PR85 and PR37) through a comparison with sea ice thicknesses estimated from the Advanced Very High Resolution Radiometer data.

The polynya boundaries and area were defined by a criterion of the monthly percentage of occurrence of thin-ice >35%. This criterion has been used in previous studies (Comiso et al., 2011; Nihashi & Ohshima, 2015; Tamura et al., 2016) and produced similar results to those obtained using a criterion of 75% of sea-ice concentration used in other studies (Massom et al., 1998; Portela et al., 2021; Xu et al., 2017). With this method, the polynya surface area changes monthly. In summer (from November to March), when most of the region is ice-free, we assigned profiles that were located within the contours of 35% of the occurrence of thin-ice between April and October of the given year. To avoid including the data off the continental shelf, data outside the contours defined by the continental slope (depths >1,500 m) were excluded from our analyses. The bathymetry for the polynya regions was obtained from RTopo-2.0.4 (Schaffer et al., 2019), (https://doi.org/10.1594/PANGAEA.905295).

2.3. Salt Budget

The deepening of the mixed layer in coastal polynyas is driven by cooling and brine rejection during sea-ice production. As the mixed layer deepens, it entrains water from below that may modify the mixed layer salinity. In order to quantify the relative contributions of brine rejection, entrainment, and salt advection to the observed monthly salinity change in each polynya, we computed a salt budget for the monthly mean mixed layer and for the interior waters below. The method is illustrated in the schematic in Figure 2.

Profiles within each month were used to compute the mixed layer depth using a potential density criterion of $\Delta\sigma_0 = 0.03$ kg m^{-3} (de Boyer Montégut et al., 2004). The mixed layer depth and salinity were then averaged in each month. Changes in salinity in each layer were calculated as the difference between consecutive monthly means.

Within the mixed layer, monthly changes in the observed salinity, ΔS_{ml}, can be decomposed as:

$$\Delta S_{ml} = \Delta S_{brine} + \Delta S_{ent} + \Delta S_{adv} \quad (1)$$

where ΔS indicates the monthly salinity change centered on day 15 of each month. Following the schematic in Figure 2, ΔS at a given month is computed as the difference between the salinity at t_2 (the average of the month 2) and at t_1 (the average of the month 1), and the subscript indicates the contributing process: S_{brine} for the salinity change due to the salt released in the mixed layer during sea-ice formation, S_{ent} for salinity change due to entrainment, and S_{adv} for lateral salt advection.

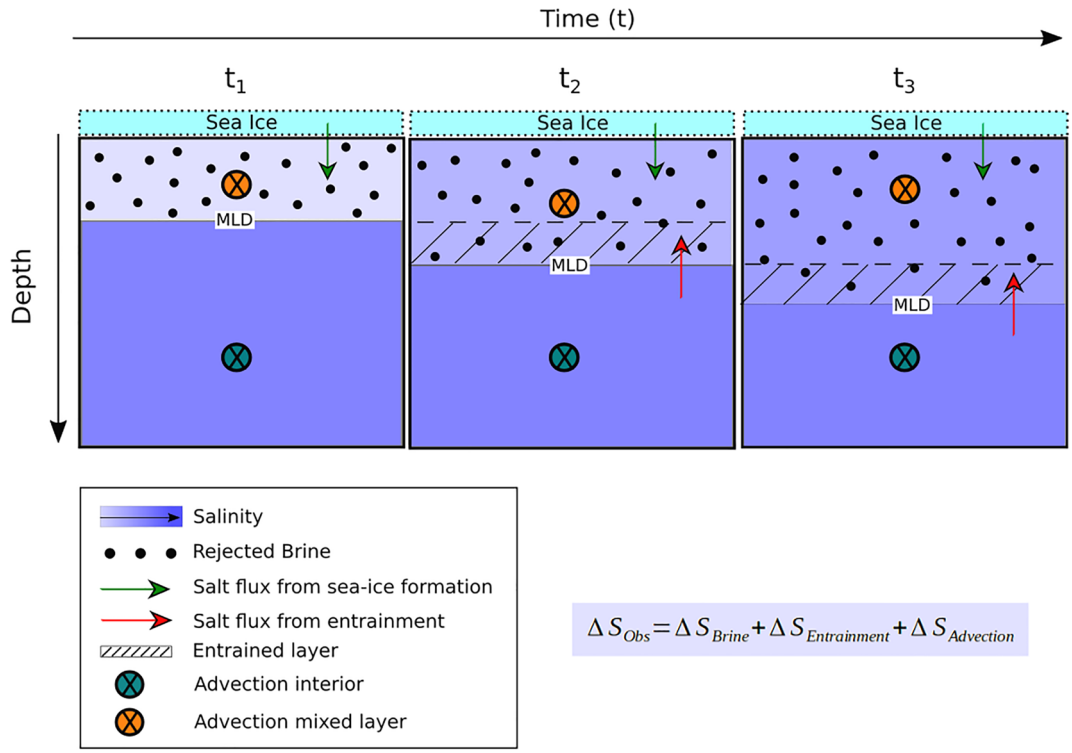

Figure 2. Schematic showing the processes considered in a salt budget computation in an Antarctic coastal polynya as driving salinity change in the mixed layer and in the interior waters below. In this example, the process is illustrated over 3 months ($t_1 - t_3$). The change in salinity from t_n to t_{n+1} (ΔS) in each case represents the mass of salt contributed by each process, divided by the volume of the mixed layer at time t_n multiplied by the density of freshwater (ρ_{fw}).

We are interested in the relative contribution of each process to the change in salinity of the mixed layer. ΔS_{brine} was obtained by first computing the monthly salt flux between t_1 and t_2 from the remotely sensed sea-ice production estimates (Sf_{SIP}), following Cavalieri and Martin (1994):

$$Sf_{SIP}(t_1 \rightarrow t_2) = \rho_i V_i(t_1 \rightarrow t_2)(S_{sw} - S_i) \quad (2)$$

where $\rho_i = 920$ kg m^{-3} is the sea ice density, V_i is the volume of sea ice formed over the polynya area in m^3, S_{sw} is the mean seawater salinity in the region, and S_i is the frazil ice salinity ($S_i = 0.31 \times S_{sw}$). (Equation 2 differs from that of Cavalieri and Martin (1994) by a factor of 10^{-3}, as we compute the salt flux in grams). For this computation, the monthly sea-ice production was accumulated from the 15th of a month to the 15th of the next month (i.e., from t_1 to t_2 in Figure 2). We then computed the salinity increase of the mixed layer at time t_2 as a result of salt added by brine release between t_1 and t_2:

$$\Delta S_{brine}(t_1 \rightarrow t_2) = \frac{Sf_{SIP}(t_1 \rightarrow t_2)}{\rho_{fw} V_{ml}(t_1)} \quad (3)$$

where ρ_{fw} is the freshwater density (1,000 kg m^{-3}), and V_{ml} is the monthly mean volume of the mixed layer.

To assess the contribution of entrainment to the salinity change in the mixed layer, we considered the following steps. The mixed layer salinity just prior to entrainment ($S_{ml}(t_2 - \epsilon)$), where ϵ represents a small amount of time is the initial salinity plus the salinity increase due to brine release:

$$S_{ml}(t_2 - \epsilon) = (SC_{ml}(t_1) + Sf_{SIP}) / \rho_{fw} V_{ml}(t_1) \quad (4)$$

where SC_{ml} is the salt content of the mixed layer. When entrainment occurs, the salinity of the mixture is:

$$S_{ml}(t_2) = (S_{ml}(t_2 - \epsilon) V_{ml}(t_1) + S_{ent} V_{ent}(t_1 \rightarrow t_2)) / V_{ml}(t_2) \quad (5)$$

21699291, 2022, 12, Downloaded from https://agupubs.onlinelibrary.wiley.com/doi/10.1029/2022JC018804 by Cochrane France, Wiley Online Library on [15/10/2024]. See the Terms and Conditions (https://onlinelibrary.wiley.com/terms-and-conditions) on Wiley Online Library for rules of use; OA articles are governed by the applicable Creative Commons License

21699291, 2022, 12, Downloaded from https://agupubs.onlinelibrary.wiley.com/doi/10.1029/2022JC018804 by Cochrane France, Wiley Online Library on [15/10/2024]. See the Terms and Conditions (https://onlinelibrary.wiley.com/terms-and-conditions) on Wiley Online Library for rules of use; OA articles are governed by the applicable Creative Commons License

where V_{ent} is the volume of the entrained layer. The salinity change due to entrainment ΔS_{ent} is then:

$$\Delta S_{ent}(t_1 \to t_2) = H\left(\frac{d(MLD)}{dt}\right)(S_{ml}(t_2) - (SC_{ml}(t_1) + Sf_{SIP})/\rho_{fw}V_{ml}(t_1)) = H\left(\frac{d(MLD)}{dt}\right)(V_{ent}(t_1 \to t_2)/V_{ml}(t_2)\ \ (S_{ent} - -S_{ml}(t_1) - -Sf_{SIP}/\rho_{fw}V_{ml}(t_1)) \quad (6)$$

where S_{ent} is the mean salinity of the entrained water and H is the unit Heaviside function which is zero for negative arguments and one for positive arguments. This function applied to the entrainment term means that if the mixed layer depth decreases from t_1 to t_2, $\Delta S_{Ent}(t_1 \to t_2)$ is set to zero.

Equation 6 provides an expression to calculate ΔS_{ent} in the general case. For the cold and nearly isothermal water column typical of Antarctic coastal polynyas, where the density stratification is almost entirely determined by salinity, the salt balance can be simplified. In this situation, entrainment will occur once the mixed layer salinity reaches that of the layer below. As the salinity of the mixed layer and the entrained layer are equal when entrainment occurs, entrainment does not change the salinity of the mixed layer. Figure S2 in Supporting Information S1 confirms that the stratification at the base of the mixed layer is nearly entirely set by salinity in the four polynyas considered here, therefore $\Delta S_{Ent} = 0$ and the expression for the change in salinity of the mixed layer can be simplified to $\Delta S_{ml} = \Delta S_{brine} + \Delta S_{adv}$. The observations of salinity and mixed layer depth are highly variable from day-to-day, reflecting irregular sampling of temporally and spatially varying fields. We therefore work with monthly means, but time-averaging can potentially introduce errors when using Equation 5 to calculate ΔS_{Ent}. We avoid introducing these errors into the analysis by setting $\Delta S_{Ent} = 0$, consistent with the physics of entrainment for a water column where the stratification is determined by salinity (Figure S2 in Supporting Information S1).

Finally, the contribution of lateral advection to the salinity change in the mixed layer (ΔS_{Adv}) was estimated as a residual, that is, ($\Delta S_{ml} - \Delta S_{brine}$). Below the mixed layer, the observed salinity change (ΔS_{int}) is only due to lateral salt advection, so:

$$\Delta S_{int_{Adv}}(t_1 \to t_2) = \Delta S_{int} = S_{int}(t_2) - S_{int}(t_1) \quad (7)$$

where S_{int} is the interior salinity computed as the mean salinity between the mixed layer base and the maximum depth each month. Observational errors, sparse seal sampling, and spatial variability could also contribute to the residual but are not taken into account in our computation. Neglecting spatial variability within polynyas might be a strong assumption since, at least in the case of MP, the water-mass distribution shows important spatial variability due to localized differences in bathymetry (Portela et al., 2021). However, for this study, most of the 2013 sampling in MP occurred over a limited area, thereby minimizing the effect of spatial variability (except in March, when the seal moved from East to West within MP). The importance of spatial variability is unknown for the other polynyas.

3. Results

The four polynyas analyzed in this study show different physiographic characteristics. All four are located next to ice shelves, but the ice shelf size, location within the bay, melt rate, and the influence of meltwater outflows from the ice shelf cavities differ. For instance, MP is situated next to the Amery ice shelf, the third largest in Antarctica, while VBP is adjacent to the smallest ice shelf considered in this study. MP and VBP both receive meltwater exported from the ice shelf cavities, which has been found to affect DSW formation there (Herraiz-Borreguero et al., 2015; Ribeiro et al., 2021; Williams et al., 2016). BP and SP are situated next to moderate-size ice shelves, the West and Shackleton ice shelves, respectively. These two ice shelves resemble ice tongues that may have multiple inflows and outflows from the ice shelf cavities, either within the polynyas or far away from them. Additionally, MP is located in western Prydz Bay, a region with a relatively wide continental shelf, while the other three polynyas are situated on narrow continental shelves and have their outer limits near the shelf break (Figure 1). Large ice shelves and wide continental shelves have been highlighted as factors favoring DSW formation by some authors (Narayanan et al., 2019), while others have recently pointed out that the presence of wide continental shelves are less important than previously thought (Amblas & Dowdeswell, 2018).

The four polynyas also differ in size: SP is the largest ($7.5 \pm 3.6 \times 10^3$ km^2), followed by VBP and BP that have similar sizes ($6.2 \pm 2.7 \times 10^3$ km^2 and $6.0 \pm 2.1 \times 10^3$ km^2, respectively) and the smallest is MP (mean

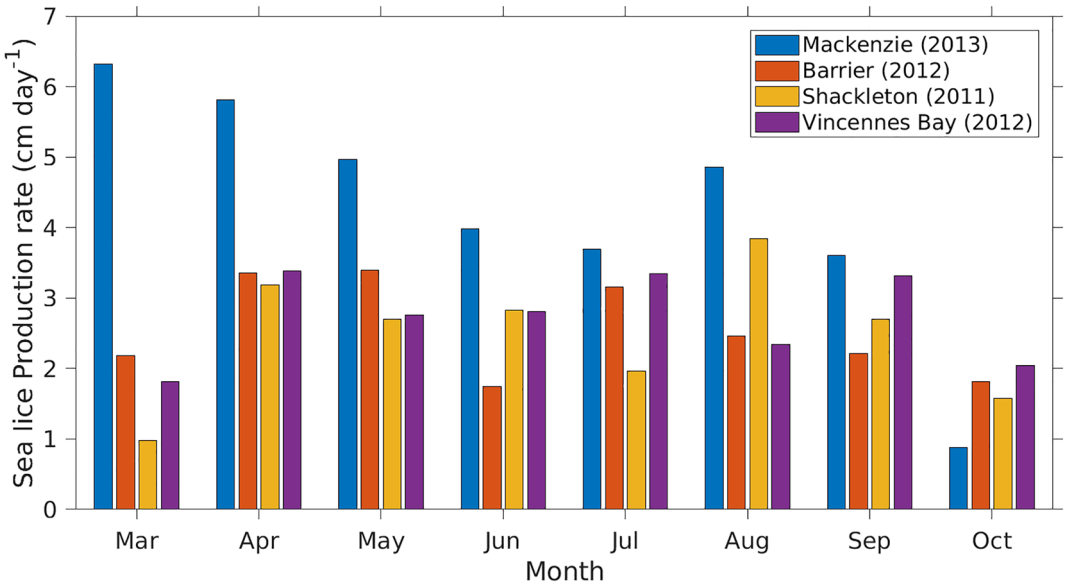

Figure 3. Monthly mean of the Sea Ice Production rate in each polynya between March and October. This average is computed over the polynyas area defined by the contours of 35% of occurrence of thin-ice (Tamura et al., 2016) as described in Section 2.2.

area $3.9 \pm 2.1 \times 10^3$ km^2). The values provided in parentheses are the mean areas reported by Nihashi and Ohshima (2015) for the period 2003–2011. In our study, mean polynya areas between May and October, computed as the integral of the grid cells with a 0.01–0.2 m thin-ice threshold are 20.1×10^3 km^2 in SP, 9.3×10^3 km^2 in BP, 8.4×10^3 km^2 in VBP and 4.5×10^3 km^2 in MP. Between March and June, all four polynyas experienced a significant size reduction, and three of them (MP, BP, and VBP) remained approximately constant until August before re-opening in September. SP exhibited different dynamics, with variable sizes throughout the winter (not shown).

3.1. Sea Ice Production

The monthly mean of the spatially averaged sea-ice production rate (Figure 3) is independent of polynya size and provides a measure of the intensity of brine rejection within each polynya. Therefore, this is the preferred parameter to assess the potential of a given polynya to form DSW, as sea-ice production is directly related to salinity increase. The sea-ice production rate is more than twice as strong in MP than in the other polynyas in March. Although the difference reduces over time, the sea-ice production rate in MP remains the highest of all four polynyas until September. Over the whole winter (between March and October, inclusive), the accumulated sea-ice production in MP is about 1.5 times larger than in the other three polynyas: 10.2 m in MP, 6.1 m in BP, 6.0 m in SP and 6.5 m in VBP.

3.2. Seasonal Water-Mass Transformation

The water mass properties in each polynya between March and October (inclusive) are shown in Figure 4 where the main water masses are labeled and the time is color-coded (see Table 1 for water mass definitions). Note that while in SP and VBP there are data from the beginning of March, in MP and BP the time series begins at the middle and the end of March, respectively (see Figure 5).

The saltiest DSW is observed in MP, with a maximum salinity of about 34.7 reached in mid-September, the end of the sampling period here (Figures 4a and 5a). A fresher variety of DSW is present in BP in September, with maximum salinity near 34.6 (Figures 4b and 5c). In contrast, no DSW is observed in SP and VBP over the period of observations, which extends until late August and November, respectively (Figures 4c, 4d and 5e, 5g). In the latter polynyas, the salinity of waters near the surface freezing point (also named Low Salinity Shelf Waters) reaches a maximum of ≈34.45 and ≈34.5, respectively.

21699291, 2022, 12, Downloaded from https://agupubs.onlinelibrary.wiley.com/doi/10.1029/2022JC018804 by Cochrane France, Wiley Online Library on [15/10/2024]. See the Terms and Conditions (https://onlinelibrary.wiley.com/terms-and-conditions) on Wiley Online Library for rules of use; OA articles are governed by the applicable Creative Commons License

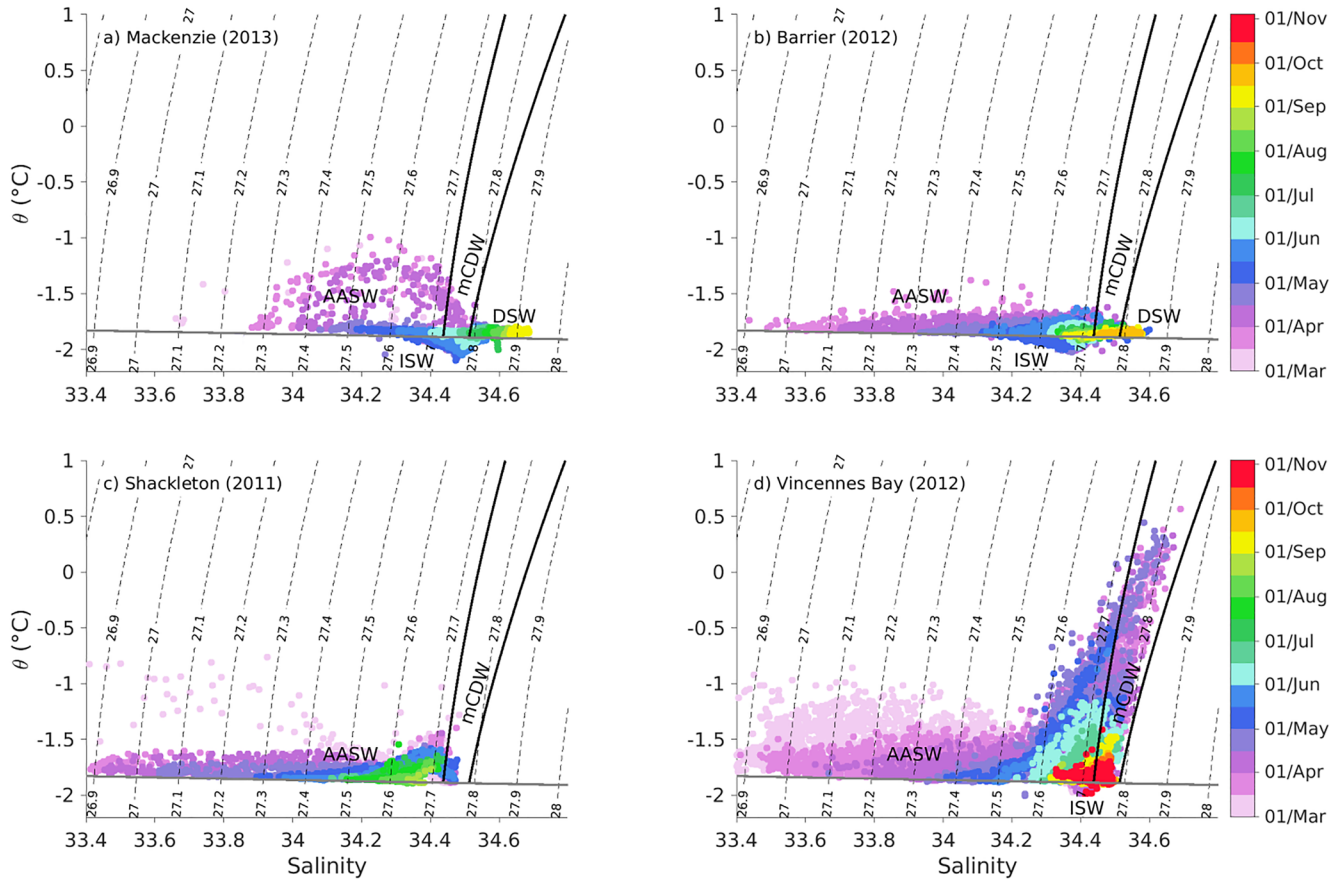

Figure 4. Potential temperature-salinity diagram in the four polynyas: (a) Mackenzie, (b) Barrier, (c) Shackleton, and (d) Vincennes Bay. The dashed lines represent the isopycnals and the thick black contours highlight the isoneutrals of 28 and 28.27 kg m^{-3} that delimit the modified Circumpolar Deep Water (mCDW). The nearly horizontal gray line is the surface freezing point. The day and month of the given years are color coded.

Besides the presence or absence of DSW, all four polynyas differ greatly in terms of water-mass distribution. mCDW is only present in MP in autumn, with a relatively cool maximum temperature of −1.5°C. mCDW was only observed when the seal sampled the eastern side of MP (Figure 1a), so it may reflect spatial variability of the water masses within the polynya (Portela et al., 2021) and Prydz Bay (Herraiz-Borreguero et al., 2015). In BP, mCDW is practically absent and only sporadically observed in SP. In contrast, mCDW is widespread and particularly warm (maximum temperatures >0.5°C) in VBP, in agreement with previous observations encompassing wider or different periods (Kitade et al., 2014; Ribeiro et al., 2021). Ice shelf water (ISW, Table 1) is present in MP and BP, the two DSW-forming polynyas, but is relatively salty/dense in MP (density ranging between 27.5 and 27.7 kg m^{-3}) compared to the fresher/lighter ISW in BP (density between 27.4 and 27.6 kg m^{-3}) (Figures 4a and 4b). ISW is absent in SP, and a relatively warm variety is observed in VBP.

Table 1
Water-Mass Classification Based on Herraiz-Borreguero et al. (2015, 2016); Williams et al. (2016) and Orsi and Wiederwohl (2009)

Water mass	Salinity	Potential temperature	Neutral density
AASW	$S < 34.4$	$\theta > T_f$	$\gamma < 28$
mCDW	–	$\theta > T_f + 0.1$	$28 < \gamma < 28.27$
ISW	–	$\theta < T_f - 0.05$	–
DSW	$S > 34.5$	$T_f - 0.05 < \theta < T_f + 0.1$	$\gamma > 28.27$

Note. AASW, Antarctic surface water; DSW, dense shelf water; mCDW, modified Circumpolar Deep Water; ISW, ice shelf water. *T_f, surface freezing point.

The properties of the Antarctic surface water (AASW), the freshest water mass of the water column, also vary between polynyas. April AASW is warmer and saltier in MP and VBP where its minimum salinity ranges between 33.8 and 34 (Figures 4a, 4d and 5a, 5g). In MP, warm AASW was only sampled in the eastern part of the polynya (Figure 1a), with different water-mass properties from the western part (Portela et al., 2021). In contrast, AASW is colder and fresher in BP and SP in April (minimum salinity of 33.4–33.5) (Figures 4b, 4c and 5c, 5e). Fresh AASW is also observed in VBP in March ($S < 33.6$). However, it rapidly becomes saltier in April ($S > 33.8$). The fresh surface layer in autumn reflects summer ice melt, and it cools and

21699291, 2022, 12, Downloaded from https://agupubs.onlinelibrary.wiley.com/doi/10.1029/2022JC018804 by Cochrane France, Wiley Online Library on [15/10/2024]. See the Terms and Conditions (https://onlinelibrary.wiley.com/terms-and-conditions) on Wiley Online Library for rules of use; OA articles are governed by the applicable Creative Commons License

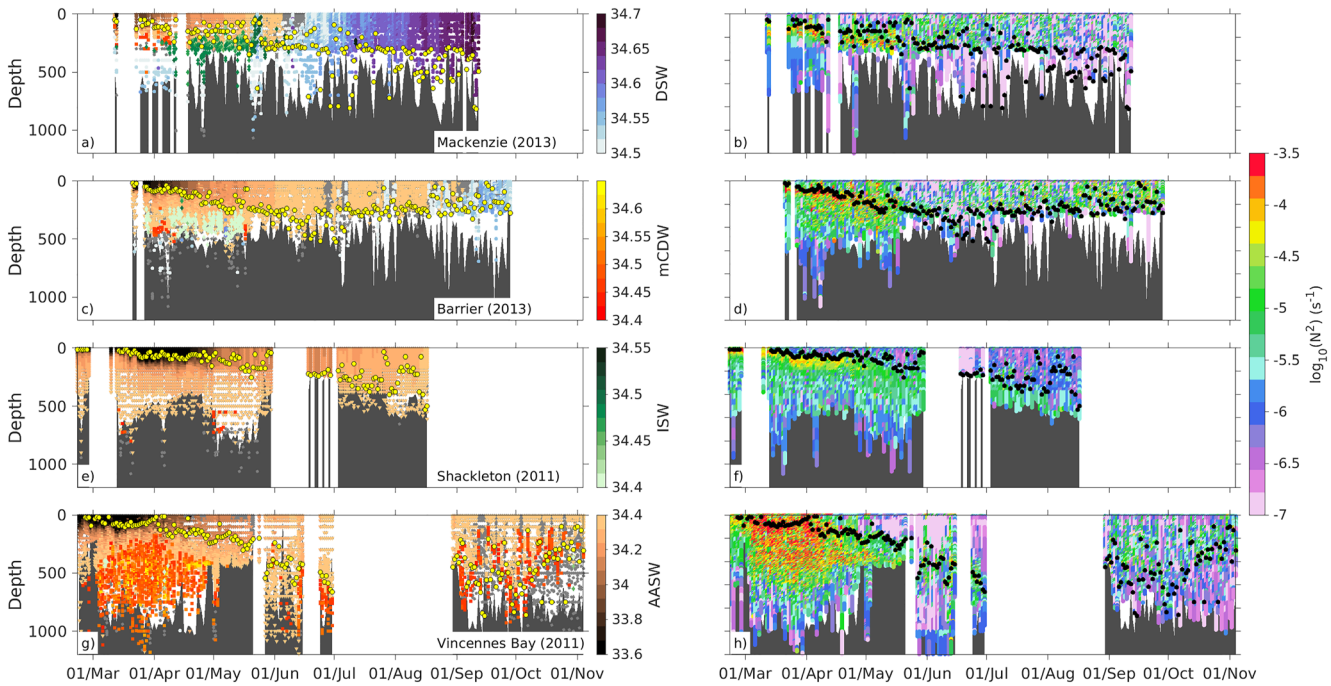

Figure 5. Time line of water column salinity (left column), highlighting the different water masses and their seasonal transformation across the four polynyas, and their stratification given by N^2 (right column). (a–b) Mackenzie, (c–d) Barrier, (e–f) Shackleton, and (g–h) Vincennes Bay. For clarity, each water mass is shown with a different color palette. Gray dots represent the transitional water masses before the minimum Dense Shelf Water (DSW) salinity is reached at a temperature near the freezing point (sometimes defined as Low Salinity Shelf Water (Gordon & Tchernia, 1972)). The yellow dots (black in right column) represent the mixed layer depth as computed with a $\Delta\sigma$ criterion of 0.03 kg m^{-3} (de Boyer Montégut et al., 2004). The bathymetry is shaded in dark gray and it represents the deepest location of all the profiles used in the daily average.

salinifies as the winter progresses. Thus, the properties of the AASW in autumn (March–April) depend on the oceanic heat loss and brine rejection in each polynya and on the amount of melt that occurred over the previous summer. Saltier (therefore denser) AASW in autumn is indicative of an earlier or more intense sea-ice production and/or less ice melt. This results in the preconditioning of the water column that would reduce stratification and favor further convection.

The vertical distribution of the water masses with time provides additional information on how they are transformed over the winter (Figures 5a, 5c, 5e and 5g, left column). In Figure 5, each water mass is represented with a different color palette. The color palette used for each water mass and their corresponding temperature and salinity features are also represented in Figure S3 in Supporting Information S1 to help the reader in the interpretation of Figure 5. To avoid over-plotting, we have used the daily average of all data available within each polynya in their particular year. This representation highlights the role of the different water masses in setting the stratification (N^2) of the water column (Figures 5b, 5d and 5f, 5h) and thus influencing the formation and evolution of DSW.

In MP, remnant DSW below the mixed layer ($S = 34.5$, blue dots in Figure 5a) is observed throughout the entire sampling period except between mid-April and mid-May, when ISW (green) is observed in the bottom layer instead. This ISW is as salty as the remnant DSW, so it is similarly dense. Full convection is achieved, and new DSW is formed in MP episodically from early June, and more consistently from July. This DSW gets progressively saltier until mid-September, the end of the sampling record (Figures 4a and 5a).

In BP, only episodic remnant DSW is found in late summer, but most of the seafloor is occupied by relatively fresh ($S = 34.4$) ISW in April and early May. Similarly, fresh mCDW is observed during the same period. Full convection is achieved in late June, but new DSW is not consistently formed until August, reaching maximum salinity of about 34.55 by the end of September (Figures 4b and 5c). In both MP and BP, the shallow bathymetry in comparison with the two other polynyas might have also contributed to achieving full convection earlier in the year.

21699291, 2022, 12, Downloaded from https://agupubs.onlinelibrary.wiley.com/doi/10.1029/2022JC018804 by Cochrane France, Wiley Online Library on [15/10/2024]. See the Terms and Conditions (https://onlinelibrary.wiley.com/terms-and-conditions) on Wiley Online Library for rules of use; OA articles are governed by the applicable Creative Commons License

21699291, 2022, 12, Downloaded from https://agupubs.onlinelibrary.wiley.com/doi/10.1029/2022JC018804 by Cochrane France, Wiley Online Library on [15/10/2024]. See the Terms and Conditions (https://onlinelibrary.wiley.com/terms-and-conditions) on Wiley Online Library for rules of use; OA articles are governed by the applicable Creative Commons License

In SP, the water column is fully occupied by AASW, except for the bottom layer (>500 m depth) which is occupied by mCDW. Despite a relatively weak stratification compared with the other polynyas (Figure 5f), full convection is never achieved and salinity by mid-August (end of the time series) remains too low to form DSW (Figures 4c and 5e). Due to data limitations, we cannot know if there was DSW formation later in the year, and the seals did not sample SP in winter in any other year.

In the relatively deep VBP embayment, the water-column structure consists of AASW overlying a thick layer of warm mCDW during the entire March to November period (with a data gap in July-August). The mixed layer deepens progressively from early April until the end of June when it reaches more than 500 m. However, by this time, full convection is not yet achieved, and mCDW still underlies AASW. By September, after the winter data gap, the mixed layer is very variable, but it does not reach the bottom of the dive profile. Despite the lack of detailed observations spanning the entire winter period, there is evidence that the mixed layer starts shallowing again by the beginning of October.

The stratification, as represented by N^2, is a measure of the stability of the water column. Therefore, weaker stratification favors full convection and DSW formation. Stratification is of similar magnitude and follows similar temporal variability in MP and BP (with a maximum slightly stronger in BP, Figure S4 in Supporting Information S1); it is slightly weaker in SP, and much stronger in VBP (Figures 5b, 5d, 5f and 5h). However, this must be interpreted in combination with the water-mass properties in order to gain insight into the processes governing DSW formation. The weaker stratification at the mixed layer base in SP between March and mid-May (Figure 5f, Figure S4 in Supporting Information S1) reflects the dominance of AASW within the water column, resulting in water properties that change more smoothly over depth. During this period, the buoyancy flux is not strong enough to induce full-depth convection in any polynya. However, from May on, the mixed layer salinity in SP is still very low, while the stratification at the base of the mixed layer is stronger than in the other polynyas. This relatively strong stratification is associated with a temperature and salinity gradient below the mixed layer (warmer and saltier AASW and some mCDW, Figure S5 in Supporting Information S1) and is most likely responsible for the absence of full convection over the winter. In BP, SP and VBP, the maximum stratification between March and May (Figure S4 in Supporting Information S1) corresponds with the abrupt vertical salinity changes associated with very fresh AASW ($S < 33.6$) occupying the mixed layer. In MP, this fresh AASW is absent, and the stratification is mainly set by the contrast between relatively salty AASW within the mixed layer and the saltier DSW or ISW below (Figure 5).

3.3. The Role of Preconditioning

Low initial salinity needs stronger transformation to achieve the threshold DSW salinity of 34.5. Therefore, the mixed layer salinity at the beginning of the winter is potentially an important factor influencing DSW formation. The difference between the salinity within the mixed layer and immediately below (another indirect measure of stratification) (Figure 6), determines the buoyancy flux needed to achieve convection.

In MP, two features favorable to DSW formation occur by early April: (a) the mixed layer waters are already relatively salty ($S \approx 34$ compared with ≈33.7 in BP, 33.85 in VBP and 33.5 in SP), (b) interior waters are saltier than in the other polynyas ($S \approx 34.4$ in MP, compared with $S \approx 34.15$ in BP and VBP, and $S \approx 33.8$ in SP). As a result, (c) in MP, the salinity of both layers converge quickly, reaching the threshold DSW salinity (34.5) by the beginning of June and increasing smoothly until September. In contrast, salinity stays constant in BP over the same period (June–September). Unfortunately, the sampling gap in VBP hinders the assessment of its seasonal transformation.

Despite the initial salinity differences between the mixed layer and below, BP, SP, and VBP all exhibit a rapid salinification during April. In MP, the salinity increase occurs at slightly lower rate in the first half of April, and then it slows down. This contrasts with the sea-ice production rate observed in MP (Figure 3a) that was notably higher than that of the other polynyas. The lower rate of salinity increase in MP in April might be related to the spatial variability of the sampling, as the seal traveled from the eastern to the western side of the polynya during this month. Our previous study highlighted important differences in water-mass properties between the eastern and western areas within MP (Portela et al., 2021). By May, the differences between polynyas have reduced. The salinity of both layers is similar in MP, BP and VBP to the beginning of July when full convection is achieved in both MP and BP (Figures 5a–5d), and the rate of salinity increase slows down in all four polynyas.

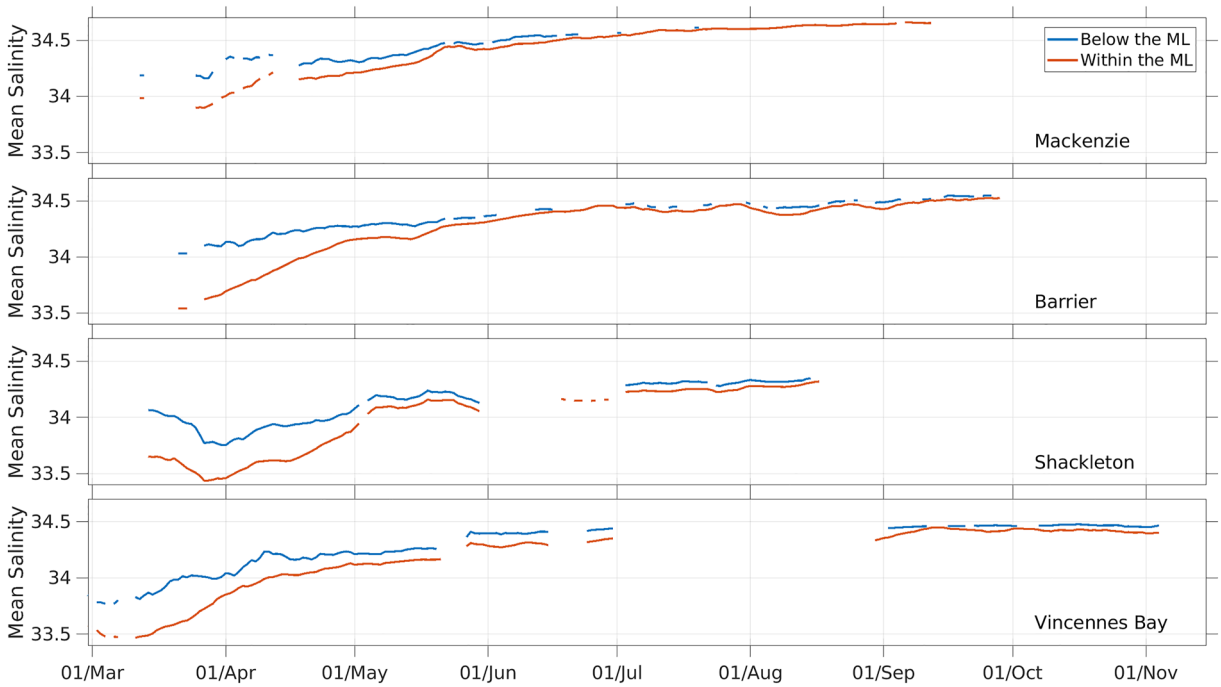

Figure 6. Temporal evolution of mean salinity within the mixed layer (red line), and within the 100 m below the mixed layer (blue line) or to the seafloor where shallower. (a) Mackenzie, (b) Barrier, (c) Shackleton, and (d) Vincennes Bay.

3.4. Salinity Balance

To better understand the processes driving the observed monthly changes in salinity, and therefore the potential for DSW formation in each polynya, we calculated two terms that could contribute to the salt balance: brine rejection due to sea-ice production, and lateral advection (as a residual), using Equations 1–7 after neglecting the entrainment term (see Methods).

In MP (Figure 7a), brine rejection from sea-ice production dominates the observed salinity increase, which is partially offset, between March and April, by the advection of relatively fresh waters within the mixed layer. The inferred advection of fresh water might reflect meltwater inflow in autumn as reported previously (Herraiz-Borreguero et al., 2015, 2016) or the transport of fresh AASW into the polynya. Salt advection also contributes to the salinity increase in the mixed layer from April to July.

Below the mixed layer, the increase in salinity with time implies positive salt advection. This could reflect an inflow of salty water masses such as mCDW or DSW. However, mCDW was not detected in MP (Figure 5a). The DSW formed in the BP may reach the MP after traveling around the Prydz Bay gyre, but the DSW produced in BP is relatively fresh. Salty DSW formed in the Cape Darnley polynya may reach the continental shelf of Prydz Bay Portela et al. (2021), but it seems unlikely that this water could flow from the outer to the inner shelf on the western side of the bay, given that the flow there is believed to run from south to north. Therefore, the increase in salinity with time below the mixed layer most likely reflects spatial variability and bathymetric influences, which were shown to strongly control water mass distributions at depth in MP (Portela et al., 2021).

In BP, the salinity increase in the mixed layer from April to June is mainly driven by salt advection, with little contribution from brine rejection as compared to MP. However, from June to September brine rejection is almost the only driver of the salinity increase, and it is completely offset by fresh advection between July and August. Based on the salinity profiles in Figure 5c, the inferred advection might reflect the inflow of relatively fresh AASW into the mixed layer once DSW has started to form.

In SP and VBP, the salinity of the mixed layer increases rapidly in autumn (Figures 7c and 7d). The increase is much larger than can be explained by SIP, implying an inflow of saltier water (either a saltier variety of AASW or mCDW). The inflow of mCDW may explain the signal in VBP, as mCDW is widespread there. In SP, mCDW is

21699291, 2022, 12, Downloaded from https://agupubs.onlinelibrary.wiley.com/doi/10.1029/2022JC018804 by Cochrane France, Wiley Online Library on [15/10/2024]. See the Terms and Conditions (https://onlinelibrary.wiley.com/terms-and-conditions) on Wiley Online Library for rules of use; OA articles are governed by the applicable Creative Commons License

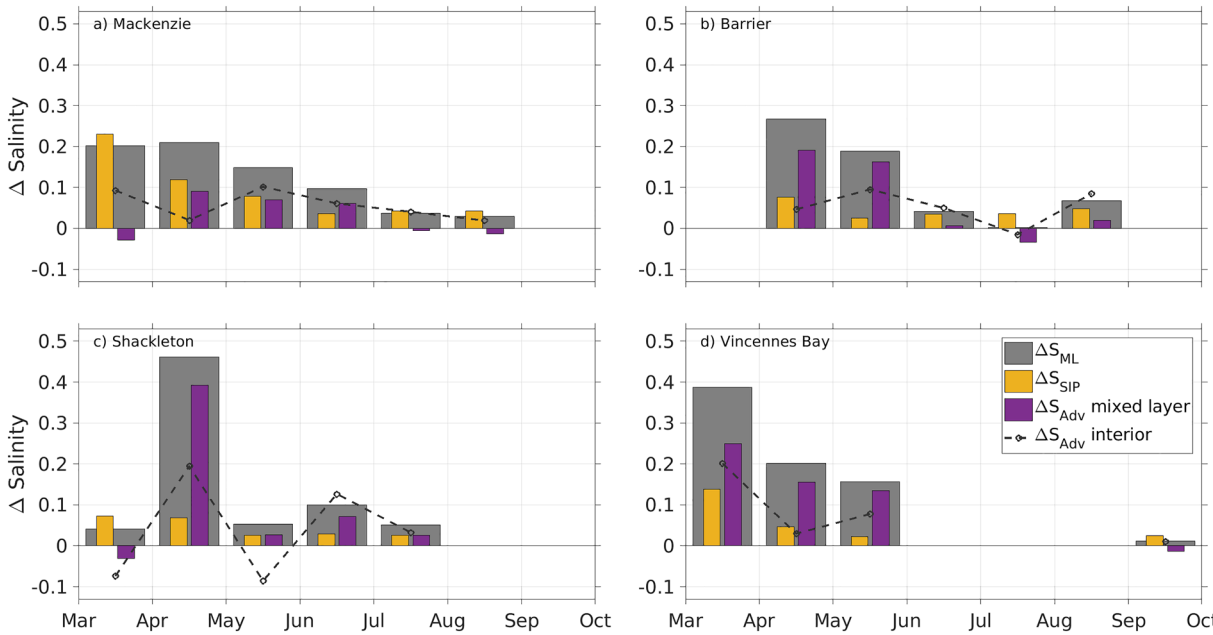

Figure 7. Monthly observed salinity increase and the relative contribution of brine rejection due to sea-ice production and advection for (a) Mackenzie (MP), (b) Barrier (BP), (c) Shackleton (SP), and (d) Vincennes Bay (VBP). The salt budget is computed within the dynamic mixed layer (bars); below the mixed layer (dashed line) the only contribution to the salinity change is advection.

rarely observed. This does not necessarily rule out a contribution from mCDW there, as rapid erosion of mCDW intrusions by mixing with AASW might dilute the signal of the former. This scenario is also consistent with the temperature increase observed in the interior AASW from April to May (Figure S5 in Supporting Information S1). From May onward, the salinity increase is small in SP (<0.1) and moderate in VBP when there is data.

The total salinity increase within the mixed layer between April and August (the common period across at least three polynyas) was 0.49 in MP, 0.50 in BP and 0.67 in SP (Figure 7). Due to the observational data gap, this cannot be assessed in the same way for VBP. The contribution of brine rejection to the salinity change over their respective records was 76% in MP, 39% in BP, 31% in SP and 30% in VBP. The fact that the total salinity increase between April and August is the smallest in MP, which forms DSW, and the largest in SP, which does not, is revealing. This suggests that a combination of factors determines whether or not DSW is formed in a given polynya, as discussed below.

4. Discussion

Here we investigated several factors influencing DSW formation in four East Antarctic polynyas with different characteristics. We analyzed the sea-ice production rate, water-mass distribution and seasonal transformation, and mixed layer depth. Using a salt budget, we estimated the relative contribution of brine rejection and salt advection to the monthly salinity change in and below the mixed layer in each polynya. The contribution of entrainment has been neglected since it is nearly zero in coastal polynyas, where the variation in temperature is small and the water column is stratified by salinity. Table 2 summarizes the characteristics of each polynya and the factors influencing DSW formation. In MP, which had the strongest DSW formation, most factors are favorable. At BP, which exhibits weak formation of lighter DSW, most factors are favorable or neutral. Conversely, most factors hinder DSW formation in SP and VBP, where DSW is not observed.

The particularly high sea-ice production rate in MP clearly favored DSW formation there. The accumulated sea-ice production over the whole winter was 1.5 times larger in MP than in the other three polynyas (Figure 3). The difference was particularly large in March when sea-ice production was strongest in MP. However, we found that DSW formation was not linked to sea-ice production alone. While sea-ice production remained high throughout the winter in MP, the increase in the mixed-layer salinity between April and August was the lowest of all polynyas (Figure 7a). The mixed layer salt budget suggests that the strong sea-ice production between March

21699291, 2022, 12, Downloaded from https://agupubs.onlinelibrary.wiley.com/doi/10.1029/2022JC018804 by Cochrane France, Wiley Online Library on [15/10/2024]. See the Terms and Conditions (https://onlinelibrary.wiley.com/terms-and-conditions) on Wiley Online Library for rules of use; OA articles are governed by the applicable Creative Commons License

21699291, 2022, 12, Downloaded from https://agupubs.onlinelibrary.wiley.com/doi/10.1029/2022JC018804 by Cochrane France, Wiley Online Library on [15/10/2024]. See the Terms and Conditions (https://onlinelibrary.wiley.com/terms-and-conditions) on Wiley Online Library for rules of use; OA articles are governed by the applicable Creative Commons License

Table 2
Summary of the Main Physiographic and Hydrographic Characteristics of Each Polynya and the Factors Evaluated in This Study

	Mackenzie	Barrier	Shackleton	Vincennes Bay
Year	2013	2012	2011	2012
Period	March–September	March–September	February–August	February–November
Area	4,500 km^2	9,300 km^2	20,000 km^2	84,000 km^2
Bathymetry	300–600	300–600	600	>1,000
DSW formation	Yes	Little	No	No
Ice shelf	Yes	Yes	Yes	Yes, small
Continental shelf	Wide	Narrow	Narrow	Narrow
DSW Remnant	Yes	Minor	No	No
Initial Salinity (Interior)	High (34.4)	Medium (34.15)	Low (33.8)	Medium (34.15)
Initial Salinity (ml)	High (34)	Medium (33.7)	Low (33.5)	Medium (33.85)
ISW	Yes, salty	Yes, fresh	No	No
mCDW	Little, early	Little, cold	Little, fresh	Strong, warm, salty
AASW	Little, cold, salty	Yes	Yes, fresh	Yes, fresh
Full convection	July	June	Never	Uncertain (August)
Stratification	Medium	Medium	Weak	Strong
Mean SIP rate (cm day^{-1})	High (4.2)	Medium (2.5)	Medium (2.5)	Medium (2.7)

Note. AASW, Antarctic Surface Water; mCDW, modified Circumpolar Deep Water; ml, mixed layer; SIP, Sea Ice Production. The green and red shading highlight conditions that favor and hinder DSW formation respectively, while yellow shading indicates neutral conditions.

and April was partially offset by fresh advection. The fresh advection likely reflects glacial meltwater entering MP from the cavity beneath the Amery Ice Shelf, which undergoes a net basal melt rate of 57.4 ± 25.3 Gt yr^{-1} (1 ± 0.4 m yr^{-1}) (Herraiz-Borreguero et al., 2016). Another possibility is that MP received an inflow of fresh AASW from neighboring areas with more sea-ice melt. However, this seems less likely given that the direction of sea ice drift was offshore (Figure S6 in Supporting Information S1).

The formation of DSW in MP was favored by the relatively high salinity observed throughout the water column from the beginning of the sampling record in March. The high salinity at the end of autumn means that less salt needs to be added to reach the salinity threshold for DSW formation. The high salinity in March could reflect (a) preconditioning of the interior waters by the presence or advection of DSW formed during the previous winter, (b) sea ice formation commencing earlier than in the other polynyas, and (c) less sea-ice melt in MP over summer. Option (a) would be consistent with the inferred advection of salty water below the mixed layer. However, this is surprising given the evidence that glacial meltwater from the Amery Ice Shelf reaches MP (Herraiz-Borreguero et al., 2016), and we argue that the apparent interior salt advection in the salt balance is an effect of the spatial variability within MP (Portela et al., 2021).

The observation that the mixed layer (i.e., AASW) salinity in MP was higher at the end of March than in the other polynyas, provides support for option (b) (sea-ice formation commencing earlier than in the other polynyas). The salinity increase in autumn in MP was also consistent with the estimated brine rejection (Figure 6). While warm surface waters in late summer can bias estimates of sea-ice production (Tamura et al., 2007), the March surface temperature approaches the freezing point in all four polynyas (Figure S5 in Supporting Information S1), providing good confidence in the sea-ice formation estimates used here.

High mixed layer salinity in MP in late autumn might also be related to less sea-ice melt over summer due to enhanced sea-ice export (option (c)). This is consistent with the strong and persistent katabatic winds blowing sea ice offshore in this region (Massom et al., 1998). To test this idea, we computed monthly sea-ice divergence in each polynya (Figure S6 in Supporting Information S1). The sea-ice velocity vectors suggest that sea-ice was

21699291, 2022, 12, Downloaded from https://agupubs.onlinelibrary.wiley.com/doi/10.1029/2022JC018804 by Cochrane France, Wiley Online Library on [15/10/2024]. See the Terms and Conditions (https://onlinelibrary.wiley.com/terms-and-conditions) on Wiley Online Library for rules of use; OA articles are governed by the applicable Creative Commons License

constantly exported from MP to the north, where there is sea-ice convergence. However, the results are inconclusive because the spatial resolution of the sea ice drift data set is insufficient to resolve polynyas.

In contrast to MP, in the other polynyas, the changes in monthly mean salinity did not track sea-ice production and lateral advection is often as large or larger than sea ice formation (Figure 7). In BP, the salinity of the mixed layer increased more rapidly from April to June than in MP, despite weaker sea ice formation, due to salt input by lateral advection. However, the initial salinity was much lower than in MP; therefore, the salinity increase through the winter was only sufficient to form a light variety of DSW. While BP and MP exhibited a number of similar characteristics (e.g., shallow bathymetry, early full convection, absence of MCDW, and similar stratification), the weaker sea ice formation and fresh conditions at the start of winter conspire to limit DSW formation in BP.

While sea-ice production rates in SP and VBP were similar to that in BP, DSW was not formed in SP and VBP. In SP, DSW formation was hindered by the presence of a thick layer of very fresh AASW from late March. One explanation for this particularly fresh AASW could be the inflow of meltwater from either the Shackleton Ice Shelf or from the Denman glacier flowing west under the Shackleton ice shelf, but we cannot corroborate this with the data in hand. The overall winter increase in mixed layer salinity was much larger at SP than at MP or BP (the data gap means this can't be assessed for VBP), despite SIP lower than MP or similar to BP, largely as a result of very strong salt advection from April to May. However, the combined salt input by brine rejection and advection was still insufficient to overcome the initial low salinity of the AASW, drive full convection, and form DSW.

VBP, like SP, showed a strong increase in mixed layer salinity at the start of the winter as a result of lateral advection (Figure 7). The mixed layer salinity in autumn in VBP was lower than at MP, but it did not have to overcome as large a mixed layer salinity deficit as at SP. However, the presence of mCDW below the surface mixed layer produced strong stratification (Kitade et al., 2014; Ribeiro et al., 2021) that provided a barrier to full-depth convection and DSW formation. At both SP and VBP, the absence of remnant DSW means that the water below the mixed layer was relatively fresh, and the salinity of the entire water column must be increased by a larger amount than at MP (and to a lesser extent, BP) to reach the threshold for DSW formation. In the case of VBP, very isolated DSW remnant samples around 500 m depth (Figure 5g) suggest that some DSW could have been formed the previous year and subsequently mixed with the ubiquitous mCDW as suggested by Kitade et al. (2014).

In addition to the hydrographic properties and the sea-ice production rate, physiographic features influenced the DSW formation in the four polynyas. MP is located on a wide continental shelf, while the other three polynyas are located on narrower shelves. Narrow continental shelves allow less time for DSW retention and salinification before the dense water cascades offshore (Amblas & Dowdeswell, 2018). The physiographic features of MP (shallow waters, wide continental shelf and presence of a large ice shelf) have been previously identified as favorable for DSW production (Amblas & Dowdeswell, 2018), although a wide shelf is not a requirement for DSW formation (Amblas & Dowdeswell, 2018; Narayanan et al., 2019). The polynya size has an influence on the total amount of DSW formed in a given polynya if the density threshold is reached. However, its relation to the sea-ice production rate is unclear; therefore, we are not taking into account the polynya size as a direct factor influencing DSW formation.

Our analysis is limited to specific years, so the presence or absence of DSW in our observations does not preclude DSW formation at a different time. Indeed, it has been shown that polynyas exhibit interannual variability (e.g., Portela et al. (2021)), especially regarding the structure of the water masses present. However, the absence of remnant DSW at SP and VBP, and the fresh waters observed at depth there, suggest that DSW either did not form in the year prior to our observations in those polynyas or it was mixed with locally dominant water masses such as mCDW in the case of VBP (Kitade et al., 2014; Ribeiro et al., 2021). In any case, our focus here is on identifying the physiographic, oceanographic and cryospheric factors that determine why DSW forms in some coastal polynyas and not others. By focusing on specific polynyas in particular years, we are able to explore in detail the factors that control DSW formation. This work therefore complements recent circumpolar assessments spanning a longer time period that investigate more general features (Amblas & Dowdeswell, 2018; Narayanan et al., 2019).

5. Concluding Remarks

We show that DSW formation in Antarctic coastal polynyas is influenced by preconditioning (e.g., salinity and stratification at the start of winter), lateral advection, and physiographic factors, as well as sea ice formation rates. By demonstrating the sensitivity of DSW formation to multiple factors, our study provides novel insights into

21699291, 2022, 12, Downloaded from https://agupubs.onlinelibrary.wiley.com/doi/10.1029/2022JC018804 by Cochrane France, Wiley Online Library on [15/10/2024]. See the Terms and Conditions (https://onlinelibrary.wiley.com/terms-and-conditions) on Wiley Online Library for rules of use; OA articles are governed by the applicable Creative Commons License

how DSW formation might respond to future changes in climate. Changes in wind strength and direction that lead to changes in polynya size and SIP are an obvious potential driver of change in DSW formation. Changes in wind forcing may also drive changes in circulation that alter the salinity and stratification of the water column (i.e., preconditioning) and hence the susceptibility to full-depth convection. Increased glacial melt will likely enhance stratification and limit DSW formation, with potential feedback on glacial melt (Silvano et al., 2018). Climate variability and change may disrupt the delicate balance of factors that control DSW formation. Previous observations and paleoceanographic evidence show that DSW formation has varied on timescales from years to millennia (de Boer et al., 2007; Smith et al., 2010). Future changes in climate are likely to alter the factors influencing DSW formation, and therefore bottom water formation and the deep overturning circulation, with important consequences for climate, ventilation of the deep ocean, and ocean-driven melt of Antarctic ice shelves.

Acronyms

MP	Mackenzie polynya
BP	Barrier polynya
SP	Shackleton polynya
VBP	Vincennes Bay polynya
DSW	Dense shelf water
AASW	Antarctic surface water
mCDW	modified Circumpolar Deep Water
ISW	Ice shelf water
AABW	Antarctic bottom water

Data Availability Statement

The marine mammal data were collected and made freely available by the International MEOP Consortium and the national programs that contribute to it (http://www.meop.net). The SSM/I data used to compute the thin-ice thickness and the sea-ice production were provided by the National Snow and Ice Data Center (NSIDC), University of Colorado (https://nsidc.org/data/nsidc-0342/versions/2).

Acknowledgments
The seal CTD-SRDL tags and deployment were funded and supported through a collaboration between the French Polar Institute (program 109: PI. H. Weimerskirch and 1201: PI. C. Gilbert and C. Guinet), the SNO-MEMO and CNES-TOSCA and the Integrated Marine Observing System (IMOS). Australia's IMOS is enabled by the National Collaborative Research Infrastructure Strategy (NCRIS). It is operated by a consortium of institutions as an unincorporated joint venture, with the University of Tasmania as Lead Agent. www.imos.org.au. The Australian Research Council provided financial support through Discovery Project DP180101667, under which E.P. is supported and through DECRA project DE180100828 under which S.B is supported. This project was also supported in part by grant funding from the Australian Government as part of the Antarctic Science Collaboration Initiative program (Australian Antarctic Program Partnership); and by the Centre for Southern Hemisphere Oceans Research, a partnership between CSIRO, the Qingdao National Laboratory for Marine Science and Technology, the University of Tasmania and the University of New South Wales. Open access publishing facilitated by University of Tasmania, as part of the Wiley - University of Tasmania agreement via the Council of Australian University Librarians.

References

Amblas, D., & Dowdeswell, J. A. (2018). Physiographic influences on dense shelf-water cascading down the Antarctic continental slope. *Earth-Science Reviews*, *185*, 887–900. https://doi.org/10.1016/j.earscirev.2018.07.014

Baines, P. G., & Condie, S. (1998). Observations and modelling of Antarctic downslope flows: A review. Ocean, ice, and atmosphere: Interactions at the Antarctic continental margin. *Antarctic Research Series*, *75*, 29–49. https://doi.org/10.1029/ar075p0029

Cavalieri, D. J., & Martin, S. (1994). The contribution of Alaskan, Siberian, and Canadian coastal polynyas to the cold halocline layer of the Arctic Ocean. *Journal of Geophysical Research*, *99*(C9), 18343. https://doi.org/10.1029/94jc01169

Comiso, J. C., Kwok, R., Martin, S., & Gordon, A. L. (2011). Variability and trends in sea ice extent and ice production in the Ross Sea. *Journal of Geophysical Research*, *116*(4), C04021. https://doi.org/10.1029/2010JC006391

de Boer, A. M., Sigman, D. M., Toggweiler, J. R., & Russell, J. L. (2007). Effect of global ocean temperature change on deep ocean ventilation. *Paleoceanography*, *22*(2), 1–15. https://doi.org/10.1029/2005PA001242

de Boyer Montégut, C., Madec, G., Fischer, A. S., Lazar, A., & Iudicone, D. (2004). Mixed layer depth over the global ocean: An examination of profile data and a profile-based climatology. *Journal of Geophysical Research: Oceans*, *109*(12), 1–20. https://doi.org/10.1029/2004JC002378

Foster, T. D., & Carmack, E. C. (1976). Frontal zone mixing and Antarctic bottom water formation in the southern Weddell Sea. *Deep-Sea Research and Oceanographic Abstracts*, *23*(4), 301–317. https://doi.org/10.1016/0011-7471(76)90872-X

Fox-Kemper, B., Hewitt, H. T., Xiao, C., Adalgeirsdottir, G., Drijfhout, S. S., Edwards, T. L., et al. (2021). Ocean, Cryosphere and Sea Level Change. In V. Masson-Delmotte, P. Zhai, A. Pirani, S. L. Connors, C. Péan, S. Berger, et al. (Eds.), *Climate Change 2021: The Physical Science Basis. Contribution of Working Group I to the Sixth Assessment Report of the Intergovernmental Panel on Climate Change*. Cambridge University Press.

Gordon, A. L., & Tchernia, P. L. (1972). Waters of the continental margin off Adélie Coast, Antarctica. Antarctic research series. *Antarctica Oceanology II: The Australian—New Zealand Sector*, *19*, 59–69. https://doi.org/10.1029/ar019p0059

Gordon, A. L., Zambianchi, E., Orsi, A., Visbeck, M., Giulivi, C. F., Whitworth, T., & Spezie, G. (2004). Energetic plumes over the western Ross Sea continental slope. *Geophysical Research Letters*, *31*(21), 5–8. https://doi.org/10.1029/2004GL020785

Herraiz-Borreguero, L., Church, J. A., Allison, I., Peña-Molino, B., Coleman, R., Tomczak, M., & Craven, M. (2016). Basal melt, seasonal water mass transformation, ocean current variability, and deep convection processes along the Amery Ice Shelf calving front, East Antarctica. *Journal of Geophysical Research: Oceans*, *121*(7), 4946–4965. https://doi.org/10.1002/2016JC011858

Herraiz-Borreguero, L., Coleman, R., Allison, I., Rintoul, S. R., Craven, M., & Williams, G. D. (2015). Circulation of modified circumpolar deep water and basal melt beneath the Amery Ice Shelf, East Antarctica. *Journal of Geophysical Research: Oceans*, *120*(4), 3098–3112. https://doi.org/10.1002/2015JC010697

Jacobs, S. S. (2004). Bottom water production and its links with the thermohaline circulation. *Antarctic Science*, *16*(4), 427–437. https://doi.org/10.1017/S095410200400224X

Jacobs, S. S., Helmer, H. H., Doake, C. S., Jenkins, A., & Frolich, R. M. (1992). Melting of ice shelves and the mass balance of Antarctica. *Journal of Glaciology*, *38*(130), 375–387. https://doi.org/10.1017/S0022143000002252

Kitade, Y., Shimada, K., Tamuta, T., Williams, G., Aoki, S., Fukamachi, Y., et al. (2014). Antarctic bottom water production from the Vincennes Bay Polynya, East Antarctica. *Geophysical Research Letters*, *41*(10), 9–13. https://doi.org/10.1002/2014GL059971

Kobayashi, T. (2018). Rapid volume reduction in Antarctic bottom water off the Adélie/George V Land coast observed by deep floats. *Deep-Sea Research Part I Oceanographic Research Papers*, *140*, 95–117. https://doi.org/10.1016/j.dsr.2018.07.014

Labrousse, S., Williams, G., Tamura, T., Bestley, S., Sallée, J. B., Fraser, A. D., et al. (2018). Coastal polynyas: Winter oases for subadult southern elephant seals in East Antarctica. *Scientific Reports*, *8*(1), 1–15. https://doi.org/10.1038/s41598-018-21388-9

Liu, C., Wang, Z., Cheng, C., Wu, Y., Xia, R., Li, B., & Li, X. (2018). On the modified circumpolar deep water upwelling over the four ladies bank in Prydz Bay, East Antarctica. *Journal of Geophysical Research: Oceans*, *123*(11), 7819–7838. https://doi.org/10.1029/2018JC014026

Malpress, V., Bestley, S., Corney, S., Welsford, D., Labrousse, S., Sumner, M., & Hindell, M. (2017). Bio-physical characterisation of polynyas as a key foraging habitat for juvenile male southern elephant seals (Mirounga leonina) in Prydz Bay, East Antarctica. *PLoS One*, *12*(9), 1–24. https://doi.org/10.1371/journal.pone.0184536

Massom, R. A., Harris, P. T., Michael, K. J., & Potter, M. J. (1998). The distribution and formative processes of latent-heat polynyas in East Antarctica. *Annals of Glaciology*, *27*, 420–426. https://doi.org/10.3189/1998aog27-1-420-426

McMahon, C. R., Roquet, F., Baudel, S., Belbeoch, M., Bestley, S., Blight, C., et al. (2021). Animal borne ocean sensors—AniBOS—An essential component of the global ocean observing system. *Frontiers in Marine Science*, *8*, 1–21. https://doi.org/10.3389/fmars.2021.751840

Narayanan, A., Gille, S. T., Mazloff, M. R., & Murali, K. (2019). Water mass characteristics of the Antarctic margins and the production and seasonality of dense shelf water. *Journal of Geophysical Research: Oceans*, *124*(12), 9277–9294. https://doi.org/10.1029/2018JC014907

Nihashi, S., & Ohshima, K. I. (2015). Circumpolar mapping of Antarctic coastal polynyas and landfast sea ice: Relationship and variability. *Journal of Climate*, *28*(9), 3650–3670. https://doi.org/10.1175/JCLI-D-14-00369.1

Ohshima, K. I., Fukamachi, Y., Williams, G. D., Nihashi, S., Roquet, F., Kitade, Y., et al. (2013). Antarctic bottom water production by intense sea-ice formation in the Cape Darnley polynya. *Nature Geoscience*, *6*(3), 235–240. https://doi.org/10.1038/ngeo1738

Orsi, A. H., Johnson, G. C., & Bullister, J. L. (1999). Circulation, mixing, and production of Antarctic bottom water. *Progress in Oceanography*, *43*(1), 55–109. https://doi.org/10.1016/S0079-6611(99)00004-X

Orsi, A. H., Smethie, W. M., & Bullister, J. L. (2002). On the total input of Antarctic waters to the deep ocean: A preliminary estimate from chlorofluorocarbon measurements. *Journal of Geophysical Research*, *107*(8), 3122. https://doi.org/10.1029/2001jc000976

Orsi, A. H., & Wiederwohl, C. L. (2009). A recount of Ross Sea waters. *Deep-Sea Research Part II Topical Studies in Oceanography*, *56*(13–14), 778–795. https://doi.org/10.1016/j.dsr2.2008.10.033

Portela, E., Rintoul, S. R., Bestley, S., Herraiz-Borreguero, L., van Wijk, E., McMahon, C. R., et al. (2021). Seasonal transformation and spatial variability of water masses within MacKenzie polynya, Prydz Bay. *Journal of Geophysical Research: Oceans*, *126*(12), 1–21. https://doi.org/10.1029/2021jc017748

Purkey, S. G., & Johnson, G. C. (2012). Global contraction of Antarctic bottom water between the 1980s and 2000s. *Journal of Climate*, *25*(17), 5830–5844. https://doi.org/10.1175/JCLI-D-11-00612.1

Ribeiro, N., Herraiz-Borreguero, L., Rintoul, S. R., McMahon, C. R., Hindell, M., Harcourt, R., & Williams, G. (2021). Warm modified circumpolar deep water intrusions drive ice shelf melt and inhibit dense shelf water formation in Vincennes Bay, East Antarctica. *Journal of Geophysical Research: Oceans*, *126*(8), 1–17. https://doi.org/10.1029/2020jc016998

Rintoul, S. R. (1998). On the origin and influence of Adélie land bottom water. Antarctic research series. *Ocean, Ice, and Atmosphere: Interactions at the Antarctic Continental Margin*, *75*, 151–171. https://doi.org/10.1029/ar075p0151

Roquet, F., Williams, G., Hindell, M. A., Harcourt, R., McMahon, C., Guinet, C., et al. (2014). A Southern Indian Ocean database of hydrographic profiles obtained with instrumented elephant seals. *Scientific Data*, *1*, 1–10. https://doi.org/10.1038/sdata.2014.28

Schaffer, J., Timmermann, R., Arndt, J. E., Rosier, S. H. R., Anker, P. G. D., Callard, S. L., et al. (2019). An update to Greenland and Antarctic ice sheet topography, cavity geometry, and global bathymetry (RTopo-2.0.4) [Dataset]. PANGAEA. https://doi.org/10.1594/PANGAEA.905295

Shapiro, G. I., Huthnance, J. M., & Ivanov, V. V. (2003). Dense water cascading off the continental shelf. *Journal of Geophysical Research*, *108*(12), 1–19. https://doi.org/10.1029/2002jc001610

Silvano, A., Rintoul, S. R., & Herraiz-Borreguero, L. (2016). Ocean-ice shelf interaction in East Antarctica. *Oceanography*, *29*(4), 130–143. https://doi.org/10.5670/oceanog.2016.105

Silvano, A., Rintoul, S. R., Peña-Molino, B., Hobbs, W. R., Van Wijk, E., Aoki, S., et al. (2018). Freshening by glacial meltwater enhances melting of ice shelves and reduces formation of Antarctic bottom water. *Science Advances*, *4*(4), 1–12. https://doi.org/10.1126/sciadv.aap9467

Silvano, A., Rintoul, S. R., Pena-Molino, B., & Williams, G. (2017). Distribution of water masses and meltwater on the continental shelf near the Totten and Moscow University ice shelves. *Journal of Geophysical Research: Oceans*, *122*(3), 2050–2068. https://doi.org/10.1002/2016JC012115

Smith, J. A., Hillenbrand, C.-D., Pudsey, C. J., Allen, C. S., & Graham, A. G. (2010). The presence of polynyas in the Weddell Sea during the last glacial period with implications for the reconstruction of sea-ice limits and ice sheet history. *Earth and Planetary Science Letters*, *296*(3–4), 287–298. https://doi.org/10.1016/j.epsl.2010.05.008

Tamura, T., Ohshima, K. I., Fraser, A. D., & Williams, G. D. (2016). Sea ice production variability in Antarctic coastal polynyas. *Journal of Geophysical Research: Oceans*, *121*(5), 1–14. https://doi.org/10.1002/2015JC011537.Received

Tamura, T., Ohshima, K. I., Markus, T., Cavalieri, D. J., Nihashi, S., & Hirasawa, N. (2007). Estimation of thin ice thickness and detection of fast ice from SSM/I data in the Antarctic Ocean. *Journal of Atmospheric and Oceanic Technology*, *24*(10), 1757–1772. https://doi.org/10.1175/JTECH2113.1

Van Wijk, E., & Rintoul, S. R. (2014). Freshening drives contraction of Antarctic Bottom Water in the Australian Antarctic Basin. *Geophysical Research Letters*, *41*, 1657–1664. https://doi.org/10.1002/2013GL058921

Williams, G. D., Bindoff, N. L., Marsland, S. J., & Rintoul, S. R. (2008). Formation and export of dense shelf water from the Adélie depression, East Antarctica. *Journal of Geophysical Research*, *113*(4), 1–12. https://doi.org/10.1029/2007JC004346

Williams, G. D., Herraiz-Borreguero, L., Roquet, F., Tamura, T., Ohshima, K. I., Fukamachi, Y., et al. (2016). The suppression of Antarctic bottom water formation by melting ice shelves in Prydz Bay. *Nature Communications*, *7*(6), 1–9. https://doi.org/10.1038/ncomms12577

Xu, Z., Gao, G., Xu, J., & Shi, M. (2017). The evolution of water property in the Mackenzie Bay polynya during Antarctic winter. *Journal of Ocean University of China*, *16*(5), 766–774. https://doi.org/10.1007/s11802-017-3286-8

21699291, 2022, 12, Downloaded from https://agupubs.onlinelibrary.wiley.com/doi/10.1029/2022JC018804 by Cochrane France, Wiley Online Library on [15/10/2024]. See the Terms and Conditions (https://onlinelibrary.wiley.com/terms-and-conditions) on Wiley Online Library for rules of use; OA articles are governed by the applicable Creative Commons License